Chapter 8
Stellar Tides

Jean-Paul Zahn

Abstract To a first approximation, a binary star behaves as a closed system; therefore it conserves its angular momentum while evolving to its state of minimum kinetic energy, where the orbits are circular, all spins are aligned, and the components rotate in synchronism with the orbital motion. The pace at which this final state is reached depends on the physical processes responsible for the dissipation of the tidal kinetic energy. For stars with an outer convection zone, the dominant mechanism is presumably the turbulent dissipation acting on the equilibrium tide. For stars with an outer radiation zone, the major dissipative process is radiative damping operating on the dynamical tide.

I shall review these physical processes, discuss uncertainties in their present treatment, describe the latest developments, and compare the theoretical predictions with the observed properties concerning the orbital circularization of close binaries.

8.1 Introduction

A fundamental property of isolated mechanical systems is that they conserve their total angular momentum while they evolve. This is true in particular for binary stars, and star-planet(s) systems, as long as one can ignore the angular momentum that is lost by the winds or by gravitational waves. Through tidal interaction, kinetic energy and angular momentum are exchanged between the rotation of the components and their orbital motion. In general, as we shall see, the system evolves toward an equilibrium state of minimum kinetic energy, in which the orbit is circular, the rotation of both stars is synchronized with the orbital motion, and their spin axes are perpendicular to the orbital plane. How rapidly the system tends to that state is determined chiefly by the strength of the tidal interaction, and therefore by the separation of the two components: the closer the system, the faster its dynamical evolution. But it also depends strongly on the efficiency of the physical processes that are responsible for the dissipation of kinetic energy into heat.

J.-P. Zahn (✉)
LUTH, Observatoire de Paris, CNRS, Université Paris-Diderot, 5 place Jules Janssen, 92195 Meudon, France
e-mail: Jean-Paul.Zahn@obspm.fr

J. Souchay et al. (eds.), *Tides in Astronomy and Astrophysics*,
Lecture Notes in Physics 861, DOI 10.1007/978-3-642-32961-6_8,
© Springer-Verlag Berlin Heidelberg 2013

Provided these dissipation processes are understood well enough, the observed properties of a binary system can deliver important information on its evolutionary state, on its past history, and even on the conditions of its formation. The first step is thus to identify these physical processes, and one may wonder why this has not been seriously undertaken until the 1990s, while the tidal theory as such had already reached a high degree of sophistication, starting with the pioneering work of Darwin [2]. The reason can be found in Kopal's classical treatise, where he declares from start that he is interested only in 'dynamical phenomena which are likely to manifest observable consequences in time intervals of the order of 10 or 100 years, and if so, tidal friction can be safely ignored' [14].

But stars live much longer than us human beings, and this is why we shall consider here changes in the properties of binary systems that span their evolutionary time scale; we shall discuss in particular the circularization of their orbits, which is both easy to observe and easy to interpret. We shall deal mainly with binary stars, although much of what follows may be applied also to star-planet systems. In the latter case, however, owing to the stark contrast between the mass of the star and that of the planet, the system may not reach the equilibrium state mentioned above, as we shall see in the next section.

8.2 Equilibrium States

To seek such equilibrium states, we follow here the method introduced by Hut [11]. Consider a binary system whose components (star or planet) are characterized by their mass (M_1, M_2), moment of inertia (I_1, I_2), and rotation vector $(\boldsymbol{\Omega}_1, \boldsymbol{\Omega}_2)$. Their orbits around the center of mass have an eccentricity e and the sum of their semi-major axes is a. The total angular momentum vector of the system is given by

$$\boldsymbol{L} = \boldsymbol{h} + I_1\boldsymbol{\Omega}_1 + I_2\boldsymbol{\Omega}_2, \tag{8.1}$$

where $\boldsymbol{h}$ designates the orbital momentum, with

$$h^2 = G\frac{(M_1M_2)^2}{M_1 + M_2}a\left(1 - e^2\right). \tag{8.2}$$

If one ignores the loss of angular momentum through winds or gravitational waves, $\boldsymbol{L}$ remains constant and it defines an inertial frame perpendicular to it; with respect to that plane, the orbital plane is inclined by an angle i. The Cartesian projections of $\boldsymbol{h}$ on the inertial frame are chosen such that

$$\boldsymbol{h} = (h\sin i, 0, h\cos i). \tag{8.3}$$

The total mechanical energy of the system (kinetic + gravitational) amounts to

$$E = -G\frac{M_1M_2}{2a} + \frac{1}{2}I_1|\boldsymbol{\Omega}_1|^2 + \frac{1}{2}I_2|\boldsymbol{\Omega}_2|^2. \tag{8.4}$$

A state of equilibrium is achieved when this E reaches a minimum under the constraint of fixed angular momentum, say $\boldsymbol{L} = \boldsymbol{L}_0$. Such a state satisfies the variational equations

$$\frac{\partial}{\partial x_i} E + \boldsymbol{\lambda} \cdot \frac{\partial}{\partial x_i} \boldsymbol{L} = 0, \tag{8.5}$$

where $\boldsymbol{\lambda} = (\lambda_x, \lambda_y, \lambda_z)$ is the Lagrangian multiplier, and where the x_i represent the nine parameters a, e, i, and $\Omega_{1,k}$, $\Omega_{2,k}$ $(k = x, y, z)$.

The next step is to derive these nine variational equations:

$$G\frac{M_1 M_2}{a} + (\lambda_x \sin i + \lambda_z \cos i)h = 0, \tag{8.6}$$

$$(\lambda_x \sin i + \lambda_z \cos i)\frac{e}{(1-e^2)}h = 0, \tag{8.7}$$

$$(\lambda_x \cos i - \lambda_z \sin i)h = 0, \tag{8.8}$$

$$\Omega_{1,k} + \lambda_k = \Omega_{2,k} + \lambda_k = 0, \quad k = x, y, z. \tag{8.9}$$

It is easy to check that this system has a unique solution, where the orbits are circular ($e = 0$), the rotation axes are perpendicular to the orbital plane ($i = 0$), and where the rotation of the two components is synchronized with the orbital motion: $\Omega_1 = \Omega_2 = \omega$, with the orbital angular velocity ω obeying Kepler's third law $\omega^2 = G(M_1 + M_2)/a^3$.

The angular momentum of these equilibrium states may be expressed as a function of the orbital frequency:

$$\mathcal{L} = \left[\frac{G^2(M_1 M_2)^3}{(M_1 + M_2)}\right]^{1/3} \omega^{-1/3} + (I_1 + I_2)\omega, \tag{8.10}$$

which has a minimum for

$$\omega^2 = \omega_{\rm cr}^2 = \left[\left(\frac{1}{3(I_1 + I_2)}\right)^3 \frac{G^2(M_1 M_2)^3}{(M_1 + M_2)}\right]^{1/2} \tag{8.11}$$

where

$$\mathcal{L} = \mathcal{L}_{\rm cr} = 4\left[\frac{(I_1 + I_2)}{27}\frac{G^2(M_1 M_2)^3}{(M_1 + M_2)}\right]^{1/4}. \tag{8.12}$$

No equilibrium state can exist below the critical value $\mathcal{L}_{\rm cr}$: for $\mathcal{L} < \mathcal{L}_{\rm cr}$ the system evolves with ever increasing orbital frequency (see Fig. 8.1), and this may eventually lead to its coalescence [11]. This occurs when the orbital angular momentum is less than 3 times the rotational angular momentum of the two components. In practice, this can only occur in very close systems, when the mass ratio is small enough:

$$\frac{M_2}{M_1} < \frac{3I_1}{M_1 R_1^2}\left(\frac{R_1}{a}\right)^2. \tag{8.13}$$

This the case for transiting planets, as was shown by Levrard et al. [20]. But here we shall deal mainly with close binary stars, for which $\mathcal{L} > \mathcal{L}_{\rm cr}$, and these will evolve towards a stable equilibrium state (located on the continuous line in Fig. 8.1).

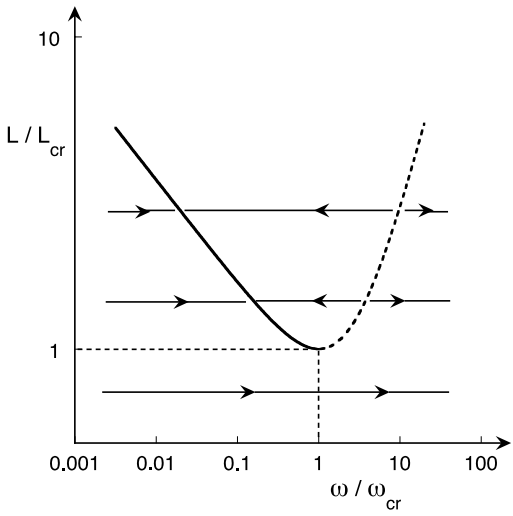

Fig. 8.1 Angular momentum of the equilibrium states of binary systems: stable equilibria are drawn in *continuous line*, unstable equilibria in *dotted line*. No equilibrium state can be achieved below the critical value $L_{\rm cr}$

8.3 The Equilibrium Tide

We begin with the most simple concept: that of the equilibrium tide, where one assumes that the star under consideration is in hydrostatic equilibrium, and that, in the absence of dissipation mechanisms, it adjusts instantaneously to the perturbing force exerted by its companion (star or planet).

8.3.1 A Crude Estimate of the Tidal Torque

For simplicity, let us assume that the orbit is circular. When the rotation of the star is synchronized with the orbital motion, the tidal bulges are perfectly aligned with the companion star; their elongation δR_1 and mass δM_1 are easily estimated, neglecting numerical factors of order unity:

$$\frac{\delta M_1}{M_1} \approx \frac{\delta R_1}{R_1} \approx \frac{(f_2 - f_1)}{GM_1/R_1^2} \approx \frac{M_2}{M_1}\left(\frac{R_1}{d}\right)^3, \tag{8.14}$$

where d is the distance between the two components, and f_1 and f_2 the forces that are exerted on the tidal bulges, as shown in Fig. 8.2. However, when the rotation is not synchronized, any type of dissipation causes a lag α of the tidal bulges, with respect to the line of centers, and the star then experiences a torque Γ which tends to drag it into synchronism:

$$\Gamma \approx (f_2 - f_1)R_1 \sin\alpha \approx -\delta M_1\left[\frac{GM_2R_1}{d^3}\right]R_1 \sin\alpha = -\frac{GM_2^2}{R_1}\left(\frac{R_1}{d}\right)^6 \sin\alpha. \tag{8.15}$$

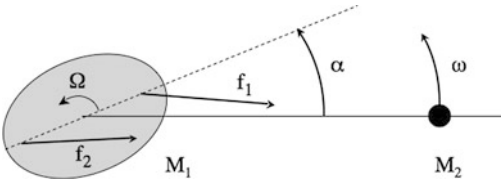

Fig. 8.2 Tidal torque. When the star under consideration rotates faster than the orbital motion ($\Omega > \omega$), its mass distribution is shifted by an angle α from the line joining the centers of the two components, due to the dissipation of kinetic energy. Since the forces applied to the tidal bulges are not equal ($f_1 > f_2$), a torque is exerted on the star, which slows it down and therefore tends to synchronize its rotation with the orbital motion ($\Omega \to \omega$)

The tidal angle α is a function of the lack of synchronism, since it vanishes for $\Omega \to \omega$, Ω being the rotation rate and ω the orbital angular velocity. In the simplest case, called the *weak friction approximation*, α is a linear function of the lack of synchronism: $\alpha = (\Omega - \omega)\delta t$, where δt is the time lag of the tidal bulge, and is thus constant in this approximation. That angle depends also on the strength of the physical process that is responsible for the dissipation of kinetic energy, which may be measured by its characteristic time $t_{\rm diss}$, with α inversely proportional to that time. This leads us to

$$\alpha = \frac{(\Omega - \omega)}{t_{\rm diss}} \frac{R_1^3}{GM_1}, \tag{8.16}$$

where we have rendered α non-dimensional by introducing the most 'natural' time, namely the dynamical (or free-fall) time $(GM_1/R_1^3)^{-1/2}$.

Inserting this expression of α in (8.15) we obtain the tidal torque

$$\Gamma = -\frac{(\Omega - \omega)}{t_{\rm diss}} q^2 M R^2 \left(\frac{R}{d}\right)^6, \tag{8.17}$$

where $q = M_2/M_1$ is the mass ratio between secondary and primary components. From here on, when there is no ambiguity, we shall drop the index 1 from R_1 and M_1.

The weak friction law (8.16) is applicable to fluid bodies, such as stars and giant planets, assuming that the dissipation is of viscous nature, and that the viscosity does not depend on the tidal frequency, namely on $(\Omega - \omega)$. (As we shall see later on, this condition is not necessarily fulfilled.) In that case the correct expression for the tidal torque, which one derives from the full equations governing the problem, is precisely of the form given above (Eq. (8.17)). From it, we may draw the synchronization time $t_{\rm sync}$:

$$\frac{1}{t_{\rm sync}} = -\frac{\Gamma}{I(\Omega - \omega)} = \frac{1}{t_{\rm diss}} q^2 \frac{MR^2}{I} \left(\frac{R}{a}\right)^6, \tag{8.18}$$

where I is the moment of inertia of the star; here the torque has been averaged over the orbit, whose semi-major axis is a. We shall see later on how the dissipation time $t_{\rm diss}$ may be evaluated.

Since the instantaneous orbital velocity varies along an elliptic orbit, so does also the torque applied to the primary. This has the effect of changing the orbital eccentricity, at a rate given by the circularization time

$$\frac{1}{t_{\rm circ}} = -\frac{d\ln e}{dt} = \frac{1}{t_{\rm diss}}\left(9 - \frac{11}{2}\frac{\Omega}{\omega}\right) q(1+q)\left(\frac{R}{a}\right)^8, \tag{8.19}$$

again in the weak friction approximation; the companion star contributes a similar amount. Note that in binary stars, synchronization proceeds much faster that circularization, because the angular momentum of the orbit is in general much larger than that stored in the stars ($I\Omega \ll Ma^2\omega$); this is not necessarily true in star-planet systems, as we have seen in Sect. 8.2. One verifies that the eccentricity decreases near synchronization, but not for fast rotation: it was Darwin [2] who first pointed out that the eccentricity actually increases when $\Omega/\omega > 18/11$.

8.3.2 *Turbulent Convection: The Most Powerful Mechanism for Tidal Dissipation*

The dissipation time $t_{\rm diss}$, which determines the tidal torque and hence the dynamical evolution of the binary system, is often treated as a free parameter, to be adjusted by the observations. We prefer to derive it from the physical processes that convert the mechanical energy of the tide into heat. The first of such processes that comes into mind is viscosity. But in stellar interiors, the viscosity due to microscopic processes is very low: it amounts typically to $\nu \approx 10$–10^3 cm^2 s^{-1}. Therefore the (global) viscous timescale R^2/ν is much longer than the age of the Universe.

Radiative damping is more efficient: the dissipation time is then of the order of the Kelvin-Helmholtz time: $t_{\rm KH} = GM/RL$, where L is the luminosity of the star. But (R/a) is raised to such a high power in (8.18) and (8.19) that $t_{\rm sync}$—and $t_{\rm circ}$ even more so—easily exceed the life-time of the star.

However viscosity still plays a key role in those regions of stars and planets that are the seat of turbulent convection. There the kinetic energy of the large scale flow that is induced by the tide cascades down to smaller and smaller scales, until it is dissipated into heat by viscous friction. The force which acts on the tidal flow may then be ascribed to a 'turbulent viscosity' of order $\nu_t \approx v_t \ell$, where v_t is the r.m.s. vertical velocity of the turbulent eddies, and ℓ their vertical mean free path (or mixing-length). The tidal dissipation time introduced in (8.18) scales as the global convective time:

$$\frac{1}{t_{\rm diss}} = \frac{6\lambda_2}{t_{\rm conv}} \quad \text{where } t_{\rm conv} = \left[\frac{MR^2}{L}\right]^{1/3}; \tag{8.20}$$

the quantity λ_2 is determined by a summation of ν_t over the whole star

$$\frac{\lambda_2}{t_{\rm conv}} = \frac{4176}{35}\pi\frac{R}{M}\int x^8 \rho \nu_t \, dx, \tag{8.21}$$

where ρ is the density and $x = r/R$ the normalized radial coordinate. This expression is approximate: it applies to a star with a thick convection zone, and it was established assuming that the whole luminosity is carried by convection [32, 44].

The convective dissipation time is very short: $t_{\rm conv} = 0.435$ yr in the present Sun, and for this reason turbulent convection is the most powerful dissipation mechanism acting on the equilibrium tide [44]. It works particularly well in stars possessing an outer convection zone, such as solar-type stars. Assuming that the whole heat flux is carried by convection and that the star is fully convective, $\lambda_2 = 0.019\alpha^{4/3}$, with α (not to be confused with the tidal lag introduced above) being the classical mixing-length parameter [47].

In stars with a convective core, tidal dissipation due to turbulent convection is considerably reduced, since it scales as $(r_c/R)^7$ with the radius r_c of that core [44]. Furthermore, in such cores the convective turnover time easily exceeds the tidal period, and therefore the straightforward definition of the turbulent viscosity taken above, i.e. $\nu_t \approx v_t \ell$, can no longer be applied, as we shall see next.

8.3.3 Which Prescription for Fast Tides?

When the local convective turnover time $t_{\rm over} = \ell/v_t$ exceeds the tidal period $P_{\rm tide}$, it seems appropriate to replace the mean free path by the distance that turbulent eddies are traveling during, say, half a tidal period. The turbulent viscosity is then given by

$$\nu_t = v_t \ell \min[1,\, P_{\rm tide}/2t_{\rm over}], \tag{8.22}$$

ignoring numerical coefficients of the order of unity [44]. This reduction occurs mainly in the deepest layers of a convection zone, since the convective turn-over time increases roughly as the 3/2 power of depth.

The same problem was addressed somewhat later by Goldreich and Nicholson [5], when they estimated the tidal damping in Jupiter. They remarked that 'though the largest convective eddies move across distances of order $\ell P_{\rm tide}/t_{\rm over}$ in a tidal period, they do not exchange momentum with the mean flow on this time scale.' Assuming that the Kolmogorov spectrum applies to convective turbulence, they retained in that spectrum only the eddies whose turnover time (or life time) is less than a tidal period; in that case, the turbulent viscosity scales as

$$\nu_t = v_t \ell \min\left[1, (P_{\rm tide}/t_{\rm over})^2\right]. \tag{8.23}$$

They concluded that 'tidal interactions between Jupiter and its satellites have played a negligible role in the evolution of the latters' orbits.'

The question of which of these prescriptions should be applied has long been considered as Achilles' heel of tidal theory. One could even question the validity of the very concept of turbulent viscosity, since we know that stratified convection is hardly a diffusive process: the transport of heat and momentum is partly achieved

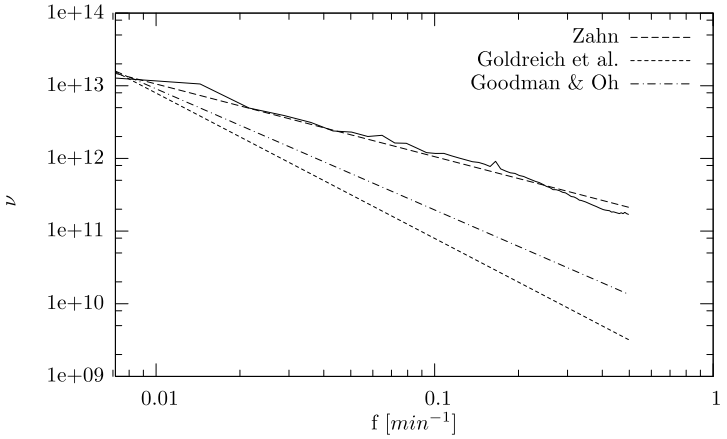

Fig. 8.3 Turbulent viscosity acting on a tidal flow in a stellar convection zone. The vertical component of that viscosity was determined by Penev et al. [30] by applying an oscillating large-scale shear on a numerical simulation of turbulent convection; it decreases with the forcing frequency f. The result (in *solid line*) is compared here with several prescriptions that have been proposed for the loss of efficiency of turbulent friction when the tidal period becomes shorter than the convective turn-over time

by long-lived plumes, and it is not easy to predict how these will interact with the large scale tidal flow.

I believe that the question will be settled through high resolution numerical simulations of turbulent convection. A first step has been taken by Penev et al. [30, 31], who studied the dissipation of a large-scale shear flow, varying periodically in time, when it is imposed on a 3-D convection simulation. They followed the method outlined by Goodman and Oh [9] to derive the viscous stress tensor. They confirmed that convection acts indeed as a turbulent viscosity on such a flow, since the off-diagonal components of the viscous tensor are one order of magnitude smaller than the diagonal components. They also observed that the vertical component of that tensor is about twice that of the horizontal components, due to the anisotropy of turbulent convection. Moreover, as can be seen in Fig. 8.3 borrowed from their article, they found that this turbulent viscosity decreases as f^{-1}, where f is the forcing frequency, which is here lower than the convective frequency. Hence they validated the first recipe (8.22) quoted above, although it remains to be seen whether their result holds in more realistic, hence more turbulent regimes.

It thus appears that turbulent dissipation operates in two regimes, depending on how the tidal period compares with the local convective turn-over time, which in a convection zone varies with depth by several orders of magnitude. To ensure a smooth transition between these two regimes, one may take

$$\nu_t = \nu_t \ell \left[1 + \left(\frac{2t_{\rm conv}}{P_{\rm tide}} \right)^2 \right]^{-1/2}, \tag{8.24}$$

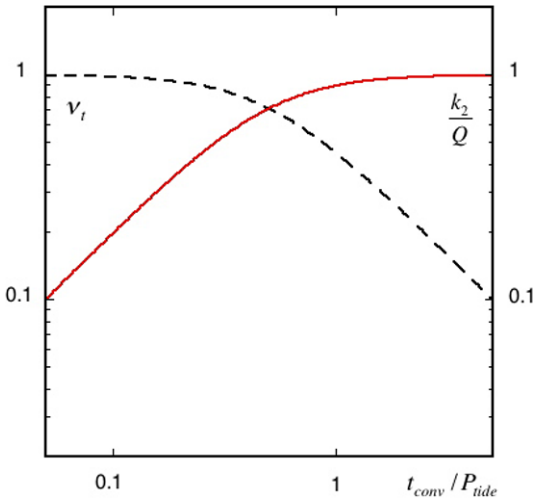

Fig. 8.4 The two regimes of turbulent dissipation (Eq. (8.24)). As long as the local convective turn-over time remains shorter than the tidal period ($t_{\rm conv} < P_{\rm tide}$), the turbulent viscosity ν_t (in *black dashed line*) is independent of the tidal frequency, and the inverse quality factor k_2/Q (in *red continuous line*) varies proportionally to the tidal frequency (σ_l) (so does also the tidal lag angle). When $t_{\rm conv} > P_{\rm tide}$, ν_t varies proportionally to the tidal period, whereas k_2/Q does no longer depend on the tidal frequency. ν_t and k_2/Q have been scaled by the value they take respectively for $t_{\rm conv}/P_{\rm tide} \to 0$ and $\to \infty$ (from Remus et al. [32], courtesy A&A)

as illustrated in Fig. 8.4. In the upper part of a convective envelope, where the convective turnover time is shorter than the tidal period, neither ν_t nor $t_{\rm diss}$ depend on the tidal period; the tidal dissipation varies proportionally to the tidal frequency (cf. Eq. (8.21)), and the tidal bulge has a constant time lag: this is what has been called the weak friction approximation [12]. But in the opposite case, when the life span of the convective eddies exceeds the tidal period, which is likely to occur at the base of convection zones, the tidal torque is independent of the tidal frequency; so are also the tidal lag angle and the quality factor Q which will be discussed next. Note that these two regimes still persist once the summation of ν_t over depth has been performed in (8.21).

8.3.4 The Quality Factor

In planetary sciences one often prefers to characterize the tidal dissipation by a dimensionless quality factor Q defined as

$$Q^{-1} = \frac{1}{2\pi E_0} \oint \left(-\frac{dE}{dt} \right) dt, \tag{8.25}$$

where E_0 is the maximum energy associated with the tidal distortion and the integral is the energy lost during one complete cycle [7]. This is equivalent to specify the tidal angle, since $\alpha = 1/(2Q)$.

This quality factor Q is always combined with the Love number k_2, which measures the mass concentration in the star; in a homogeneous body $k_2 = 3/2$. In fluid bodies, such as stars with convection zones or giant planets, the tidal torque is given by a summation over the star of the turbulent viscosity, as we have seen above in Sect. 8.3.2, and Q is related to the coefficient λ_2 we have introduced there (Eq. (8.21)):

$$\frac{k_2}{Q} = 4\frac{\lambda_2}{t_{\rm conv}}\left(\frac{R^3}{GM}\right)(\omega - \Omega). \tag{8.26}$$

Usually Q is treated as a positive quantity, and the sign of the tidal torque is imposed according to that of $(\omega - \Omega)$.

We see that the quality factor Q depends both on intrinsic properties of the star (or the planet) and on the degree of synchronism, and this fact is often overlooked when comparing the Q of different planets or satellites in the solar system. If, as it has been suggested (cf. [29]), the circularization period of late-type binary stars is roughly consistent with $Q = 10^6$, it means that λ_2 is inversely proportional to the tidal frequency $(\omega - \Omega)$, hence that the turbulent viscosity is reduced according to the first prescription (8.22). If one chooses instead the quadratic reduction (8.23), as done in the paper quoted above, Q scales as the tidal frequency.

8.3.5 Beyond the Weak Friction Approximation

When the turbulent viscosity depends on the tidal period, the weak friction approximation no longer applies, and Hut's elegant method can no longer be applied to determine the tidal torque. It is then necessary to break the tidal potential in its multiple Fourier components, of frequencies $\sigma = (j\omega - m\Omega)$, and to sum up the torques exerted by each of these. Keeping only the second order spherical harmonics of the potential, and up to second order terms in eccentricity e, which is sufficient for many purposes, one has

$$\begin{aligned} U = \frac{GM_2}{a}\left(\frac{r}{a}\right)^2 \Bigg\{ & -\frac{1}{2}P_2(\cos\theta)\left[1 - \frac{3}{2}e^2 + 3e\cos\omega t + \frac{9}{2}e^2\cos 2\omega t\right] \\ & + \frac{1}{4}P_2^2(\cos\theta)\left[-\frac{e}{2}\cos(\omega - 2\Omega)t + \left(1 - \frac{5}{2}e^2\right)\cos(2\omega - 2\Omega)t\right. \\ & \left. + \frac{7e}{2}\cos(3\omega - 2\Omega)t + 17\frac{e^2}{2}\cos(4\omega - 2\Omega)t\right]\Bigg\}. \end{aligned} \tag{8.27}$$

Each component of the tidal potential produces a tidal flow of frequency $\sigma = [j\omega - m\Omega]$, which experiences a different turbulent viscosity ν_t, since it depends on the tidal frequency (cf. Sect. 8.3.3). This is reflected in the coefficient λ_2 introduced

above in (8.21), which takes a different value $\lambda^{m,l}$ for each tidal frequency. In a star with a deep outer convection zone, such as a late-type main-sequence star or a red giant, this parameter varies approximately as

$$\lambda^{m,l} = 0.019\alpha^{4/3}\left(\frac{3160}{3160+\eta^2}\right)^{1/2} \quad \text{with } \eta = [j\omega - m\Omega]t_{\rm conv}, \tag{8.28}$$

where $t_{\rm conv}$ is given in (8.21) and α is the familiar mixing-length parameter.

The equations governing the orbital evolution of the binary system then take the following form, to second order in e and assuming for simplicity that all spins are aligned [47]:

$$\begin{aligned}\frac{d\ln a}{dt} = -\frac{12}{t_{\rm conv}}q(1+q)\left(\frac{R}{a}\right)^8\Bigg(&\lambda^{2,2}\left[1-\frac{\Omega}{\omega}\right]\\ &+e^2\left\{\frac{3}{8}\lambda^{0,1}+\frac{1}{16}\lambda^{2,1}\left[1-2\frac{\Omega}{\omega}\right]\right.\\ &\left.-5\lambda^{2,2}\left[1-\frac{\Omega}{\omega}\right]+\frac{147}{16}\lambda^{3,2}\left[3-2\frac{\Omega}{\omega}\right]\right\}\Bigg),\end{aligned} \tag{8.29}$$

$$\begin{aligned}\frac{d\ln e}{dt} = -\frac{3}{t_{\rm conv}}q(1+q)\left(\frac{R}{a}\right)^8&\\ \times\left(\frac{3}{4}\lambda^{0,1}-\frac{1}{8}\lambda^{2,1}\left[1-2\frac{\Omega}{\omega}\right]-\lambda^{2,2}\left[1-\frac{\Omega}{\omega}\right]+\frac{49}{8}\lambda^{2,3}\left[3-2\frac{\Omega}{\omega}\right]\right),&\end{aligned} \tag{8.30}$$

plus similar contributions of the secondary star (we recall that $q = M_2/M_1$). Note that we have added here the contribution of the axisymmetric part of the perturbing potential (which varies also in time when the orbit is eccentric, and yields the term in $\lambda^{0,1}$). The angular velocity of the primary star obeys

$$\begin{aligned}\frac{d}{dt}(I\Omega) = \frac{6}{t_{\rm conv}}q^2MR^2\left(\frac{R}{a}\right)^6\Bigg(&\lambda^{2,2}[\omega-\Omega]\\ &+e^2\left\{\frac{1}{8}\lambda^{2,1}[\omega-2\Omega]-5\lambda^{2,2}[\omega-\Omega]+\frac{49}{8}\lambda^{2,3}[3\omega-2\Omega]\right\}\Bigg),\end{aligned} \tag{8.31}$$

and likewise for the secondary star. One verifies that the total angular momentum is conserved, i.e. that

$$\frac{d}{dt}\left[\frac{GM_1M_2}{(M_1+M_2)^{1/2}}a^{1/2}\left(1-e^2\right)^{1/2}+I_1\Omega_1+I_2\Omega_2\right] = 0. \tag{8.32}$$

Equation (8.32) reduces to (8.18) and (8.31) to (8.19) when all $\lambda^{m,j} \to \lambda_2$, in the weak friction approximation.

8.4 Confronting the Theory of the Equilibrium Tide with the Observations

Having identified the most efficient dissipation mechanism, namely turbulent convection acting on the equilibrium tide, we shall now examine how well it accounts for the observed properties in binary stars involving at least one component possessing an outer convection zone. We shall treat in turn the case of solar-type binaries on the main-sequence, that of such binaries during their pre-main sequence phase, and finally that of binaries in which one component has evolved to the giant stage.

8.4.1 Solar-Type Binaries on the Main Sequence

Applying Eq. (8.19) to a binary of equal components of solar mass and age $t_{\rm age}$, one finds that its orbit should be circular if its period is less than about

$$P_{\rm circ} = 6\left(\frac{t_{\rm age}}{5\ {\rm Gyrs}}\right)^{3/16} \ {\rm days}. \tag{8.33}$$

To obtain this result we assume that the rotation is synchronized with the orbital motion, and that the eccentricity decreased from $e = 0.30$, a typical value for non-circularized binaries, to $e = 0.02$, taken as detection threshold for the eccentric orbits.

Koch and Hrivnak [13] were the first to compare this theoretical prediction with the distribution $e(P)$ of field binaries drawn from Batten's catalogue of spectroscopic binaries, and they found them to be compatible, although the transition period $P_{\rm circ}$ between circular and elliptic orbits was rather poorly defined, as one may expect with such a sample mixing stars of different mass and age.

But the fact that the transition period is a slowly increasing function of age should be observable, by measuring the eccentricity of coeval cluster binaries. Such a trend was found indeed by comparing the results of several surveys [3, 17, 26]. This incited Mathieu and Mazeh [21] to suggest that the determination of $P_{\rm circ}$ could serve to evaluate the age of a cluster. However for M67, a cluster of about solar age, they found that the transition period was between 10.3 and 11 days, well above the predicted 6 days, suggesting that tidal dissipation was about 20 times more efficient than inferred from the mixing-length theory.

Recently Mathieu et al. [22] gave a summary of the beautiful work accomplished over more than a decade by several dedicated teams (Fig. 8.5). They found that the transition period for circularization increases with age beyond 1 Gyr, but that it is more or less constant for younger stars, around $P_{\rm circ} \approx 7$–8 days. It thus appears that two different mechanisms are at work, one operating on old binaries, and another that circularizes the young binaries even on the PMS.

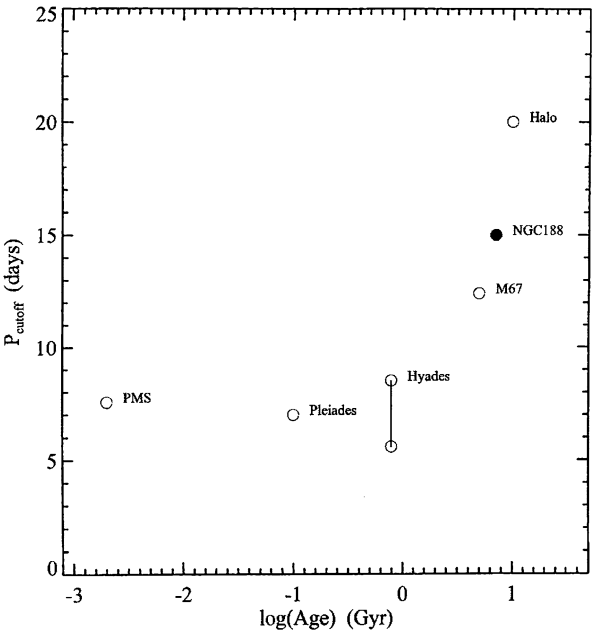

Fig. 8.5 Transition periods for circularization, below which the binary orbits are circularized, are displayed vs. age for six coeval stellar samples: PMS [25], Pleiades [26], Hyades [3], M67 [17], NGC 188 [22] and Galactic halo stars [18]. Note the near constancy of this period below 1 Gyr, at about $P_{\rm circ} \approx 8$ days, and its increase with age beyond. (From Mathieu et al. [22]; courtesy ApJ)

8.4.2 *Orbital Circularization During the Pre-Main-Sequence Phase*

The rate at which orbits are circularized depends strongly on the radius of the star: according to (8.19) $-d \ln e/dt \propto R^8$. Therefore one expects that most of this circularization should occur on the PMS, where the stellar radius is much larger than later on the main-sequence. This suggestion was first made by Mayor and Mermilliod [23], and I verified it with L. Bouchet by integrating Eqs. (8.30)–(8.32) which describe the tidal evolution of solar-type binaries, starting at the birthline defined by Stahler [36, 37]. Since on the PMS the convective turnover time can exceed the orbital period, it will also exceed the period of most Fourier components present in the tidal perturbation (cf. (8.28)), and therefore one must take into account the reduction of the turbulent viscosity, as was discussed in Sect. 8.3.5.

The result is displayed in Fig. 8.6, for a binary consisting of two solar-mass stars. The initial conditions were taken as $R = 4.79 R_\odot$, $e = 0.3$, $(\Omega/\omega) = 3$, and the orbital period P was chosen such that the eccentricity would drop to 0.005 when the binary reaches the zero age main-sequence (ZAMS). The rotation quickly synchronizes with the orbital motion (in less than 10^5 yrs), but thereafter the tidal torque weakens because the convection zone retreats, while the star keeps contracting; therefore the rotation speeds up again to about $(\Omega/\omega) = 2$ at the ZAMS, with our choice of initial conditions. Once the star has settled on the MS, synchronization proceeds unhindered, and is achieved by an age of 1 Gyr. The eccentricity first increases, as long as $(\Omega/\omega) > 18/11$ (cf. Eq. (8.19)), and then it steadily decreases

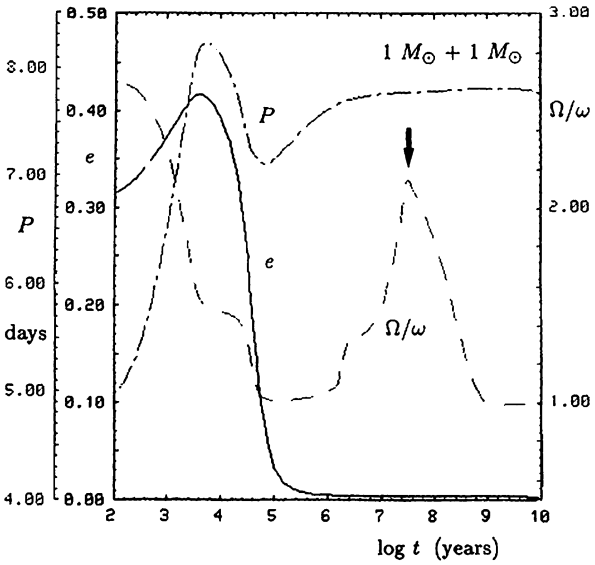

Fig. 8.6 Evolution in time of the eccentricity e, the orbital period P and of the ratio between rotational and orbital frequencies (Ω/ω), for a system with two components of 1 $M_\odot$. The initial period has been chosen such that the eccentricity would decrease from 0.300 to 0.005 when the binary reaches the zero age main-sequence (indicated by the *arrow*). (From Zahn and Bouchet [49]; courtesy A&A)

to reach its final value $e = 0.005$ at the ZAMS. Little circularization occurs thereafter on the MS. Angular momentum is transferred from the rotation to the orbit, which explains why the orbital period increases from 5 to 7.8 days. This final period depends rather weakly on the mass of the components, and it represents thus the transition period for circularization, in the absence of other tidal braking mechanisms.

This transition period agrees remarkably well with the properties of late type binaries younger than 1 Gyr, including the PMS stars, and thus there is little doubt that the circularization in these stars is due to the action of the equilibrium tide early on the PMS. The main uncertainties in the theoretical prediction are the initial radius R_i ($P_{\rm circ}$ scales as R_i to the power 15/16) and the recipe used to reduce the turbulent viscosity when the tidal period becomes shorter than the convective turnover time. We took here the linear prescription (8.22); with the other, quadratic prescription (8.23) the predicted transition period would be substantially shorter, contrary to what is observed.

It is important to note that binaries in their early MS stage may be circularized while still not synchronized, which may seem paradoxical since the synchronization time (8.18) is much shorter than the circularization time (8.19). It stresses the necessity of following the whole tidal evolution of a given binary, starting from 'reasonable' initial conditions.

8.4.3 Circularization of Binaries Evolving off the Main-Sequence

Another clever test for the tidal theory was performed by Verbunt and Phinney [40], who chose for that a sample of wide binaries containing a giant star, because they

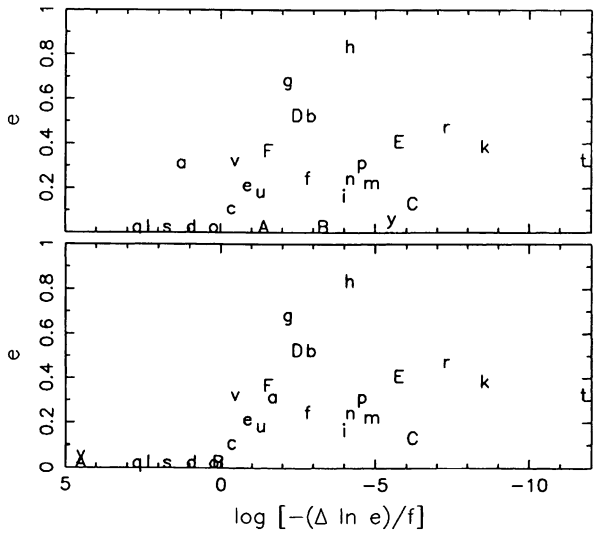

Fig. 8.7 Observed eccentricities of binaries including a giant component vs. the change in eccentricity predicted by the tidal theory, invoking the equilibrium tide with turbulent dissipation in the convection zone (Verbunt [40], courtesy A&A). In the *upper panel* the giant components are assumed to be on the asymptotic giant branch; some corrections have been applied to obtain the result of the *lower panel* (see text)

wanted to avoid what they call the 'troublesome problem of pre-main sequence circularization' that we just discussed. Moreover, in such binaries the tidal period exceeds the convective turnover time, so that there is no need to worry about reducing the turbulent viscosity. They considered 29 binaries with giant components in several galactic clusters, whose age and distance are well established. They integrated the circularization equation (8.19) for these binaries from the MS to their present location in the HR diagram, and presented the result in the form $-\Delta \ln e/f$, where $\Delta \ln e$ is the change in eccentricity, and f a factor that depends on the convection theory used to calculate the turbulent dissipation. For the classical mixing-length treatment that was employed in Sect. 8.3.2, f is of order unity.

Figure 8.7 displays the *observed* eccentricity of these binaries (each individually labeled by a letter) as a function of the *predicted* drop in eccentricity $-\Delta \ln e$ (or rather $\log[-\Delta \ln e/f]$ to accommodate the wide range of results). For $\log[-\Delta \ln e/f] > 0$), the orbit should be circularized, whereas it should remain elliptic for $\log[-\Delta \ln e/f] < 0$. Phinney and Verbunt first assumed that all their binaries are presently on the asymptotic giant branch (core helium burning), because they stay there 10 times longer than previously on the red giant branch (shell hydrogen burning).

The result is shown in the upper panel: the great majority of binaries complies with the theoretical prediction, displaying circular orbits for $\log[-\Delta \ln e/f] > 0$ and eccentric obits for $\log[-\Delta \ln e/f] < 0$. However there are 4 notable exceptions: binary 'a' has kept an eccentricity of 0.30, while its orbit should still be circular, and binaries 'A', 'B', 'y' have circular orbits, where these should be elliptic. Phinney and Verbunt concluded that binary 'a' must still be ascending the red giant branch, thus avoiding circularization, and that the other 3 binaries may have undergone an exchange of matter, which very efficiently circularizes the orbit, and therefore that they should have an evolved companion, such as a white dwarf. After these adjust-

ments, the 4 binaries are no longer exceptions, as can be seen in the lower panel; moreover, the fact that the transition from circular to elliptic orbits occurs in the vicinity of $\log[-\Delta \ln e/f] \approx 0$ confirms that the parameter f is indeed of order unity, thus validating the theory of the equilibrium tide with turbulent dissipation.

Two years later Landsman et al. [16] announced that the secondary of S1040 in M67, the binary labeled 'A', is indeed a white dwarf, confirming the brilliant conjecture of Verbunt and Phinney that it must have experienced an episode of mass exchange.

We may thus conclude that turbulent viscosity acting on the equilibrium tide explains most observations, with the important exception of the circularization of main-sequence binaries older than about 1 Gyr, for which it seems that we have to seek another dissipation mechanism. A plausible candidate for that is the dynamical tide, which we shall examine next.

8.5 The Dynamical Tide

Due to its elastic properties, a star can oscillate in various modes: acoustic modes, internal gravity modes, inertial modes, where the restoring force is respectively the compressibility of the gas, the buoyancy force in stably stratified regions, and the Coriolis force in the rotating star. If their frequency is low enough, these modes can be excited by the periodic tidal potential; the response is called the *dynamical tide*.

8.5.1 Gravity Modes Excited by a Close Companion

The modes that have received most attention so far are the tidally excited gravity modes; associated with radiative damping, they have first been invoked for the tidal evolution of massive main-sequence binaries [45]. For these modes, the restoring force is provided by the buoyancy, whose strength is measured by the buoyancy frequency N, given by

$$N^2 = \frac{g\delta}{H_P}\left[\left(\frac{\partial \ln T}{\partial \ln P}\right)_{\rm ad} - \frac{d\ln T}{d\ln P} + \frac{\varphi}{\delta}\frac{d\ln \mu}{d\ln P}\right], \tag{8.34}$$

using classical notations, and μ being the molecular weight ($\delta = -(\partial \ln \rho/\partial \ln P)_{T,\mu}$ and $\varphi = (\partial \ln \rho/\partial \ln \mu)_{T,P}$ are unity for perfect gas).

The modes that are most excited are those whose frequency is close to the tidal frequency, and these are of high radial order: typically they have more than 10 or 20 radial nodes in the radiation zone, because their wavelength scales as $\lambda_r \propto r\sigma/N$, and because the tidal frequency σ, of the order of days^{-1}, is much lower than the buoyancy frequency N, of the order of 1 hour^{-1}. See Fig. 8.8 for a typical example of such modes, in a 4 $M_\odot$ star of 94 Myr. Dissipation has been neglected, and therefore the mode is an adiabatic standing wave; note that it is evanescent in the convective core, where $N^2 \approx 0$.

These gravity modes couple with the periodic tidal potential in the vicinity of the convective core, whereas their damping occurs mainly near the surface, because the

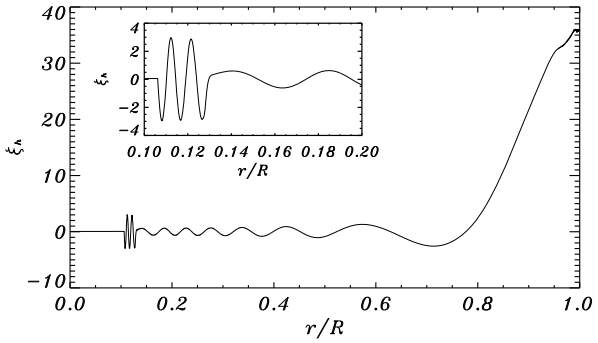

Fig. 8.8 Gravity mode of period 4 days in a 4 $M_\odot$ star of 94 Myr. Only the horizontal displacement ξ_h is shown, scaled such that the radial component $\xi_r = 1$ at the surface; it has 20 radial nodes. The *insert* focuses on the region close to the convective core, where the eigenfunction displays strong oscillations due the steep composition gradient. The effect of rotation is neglected (from Hasan et al. [10], courtesy A&A)

thermal damping rate, which scales roughly as the cube of the temperature, is much higher there than in the deep interior. The angular momentum drawn from the orbit is deposited near the surface, and hence it is the surface layers that are synchronized first with the orbital motion. As was emphasized by Goldreich and Nicholson [6], this synchronization is further sped up because the local tidal frequency experienced by the fluid entrained in the differential rotation, $\sigma = 2\Omega(r) - 2\omega$, tends to zero, and so does also the radial wavelength λ_r, as we have seen above, thus enhancing the damping.

At low enough tidal frequency, the tidal wave is completely damped (meaning that is has become a pure propagating wave), and one can use the WKB treatment to evaluate the total torque applied on the star [45]. For the synchronization time (assuming uniform rotation) one finds

$$\frac{1}{t_{\rm sync}} = -\frac{d}{dt}\left|\frac{2(\Omega-\omega)}{\omega}\right|^{-5/3} = 5\left(\frac{GM}{R^3}\right)^{1/2} q^2(1+q)^{5/6}\frac{MR^2}{I}E_2\left(\frac{R}{a}\right)^{17/2}, \tag{8.35}$$

and likewise for the circularization time, assuming that synchronization has already been achieved:

$$\frac{1}{t_{\rm circ}} = -\frac{d\ln e}{dt} = \frac{21}{2}\left(\frac{GM}{R^3}\right)^{1/2} q(1+q)^{11/6}E_2\left(\frac{R}{a}\right)^{21/2}; \tag{8.36}$$

the companion star contributes a similar amount. E_2 is a parameter measuring the coupling between the tidal potential and the gravity mode: it depends sensitively on the size of the convective core, and thus on the mass of the star. Its expression is given in Zahn [45]; it has been tabulated by Claret and Cunha [1] for various stellar models, as shown in Fig. 8.9; for a 10 $M_\odot$ ZAMS star, it is $E_2 \approx 10^{-6}$.

This theory was initially developed for pure gravity modes, and as such it was strictly applicable only to non-rotating stars. It was later extended by Rocca [34]

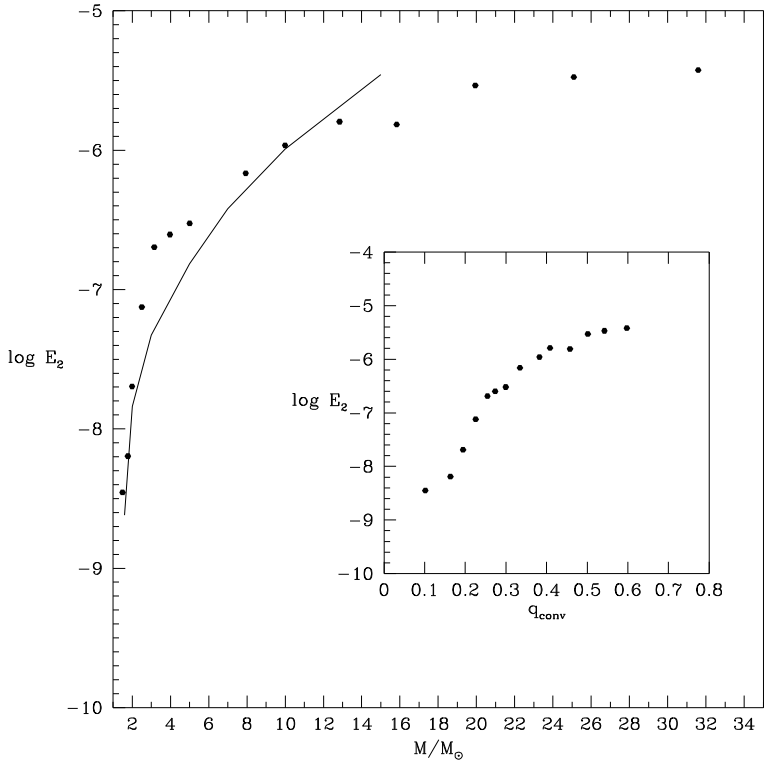

Fig. 8.9 Tidal parameter E_2 characterizing the strength of the dynamical tide, cf. (8.35) and (8.36). It is displayed here on a logarithmic scale, as a function of mass (in solar units), near the ZAMS. The *solid line* reports the results of earlier computations by Zahn [45]. The *insert* shows the dependence of E_2 on the relative size of the convective core (from Claret and Cunha [1]; courtesy A&A)

to (uniformly) rotating stars; she showed that taking the Coriolis force into account modifies only slightly the results presented above.

8.5.2 Circularization of Massive Binaries

Giuricin et al. [4] were the first to compare the predictions of the tidal theory with the properties of early-type binaries, thus possessing an outer radiation zone. Applied to binaries with two identical components of mass between 2 and 15 $M_\odot$, Eq. (8.36) predicts a transition value of $R/a \approx 0.25$ for the normalized radius, i.e. the radius expressed in units of semi-major axis.[1] This value is in good agreement with the

[1]This value depends little on mass [46]; if it were translated into tidal periods, the transition periods would spread between 1 to 2 days, depending on mass, which explains why it is preferable to use R/a for the observational test.

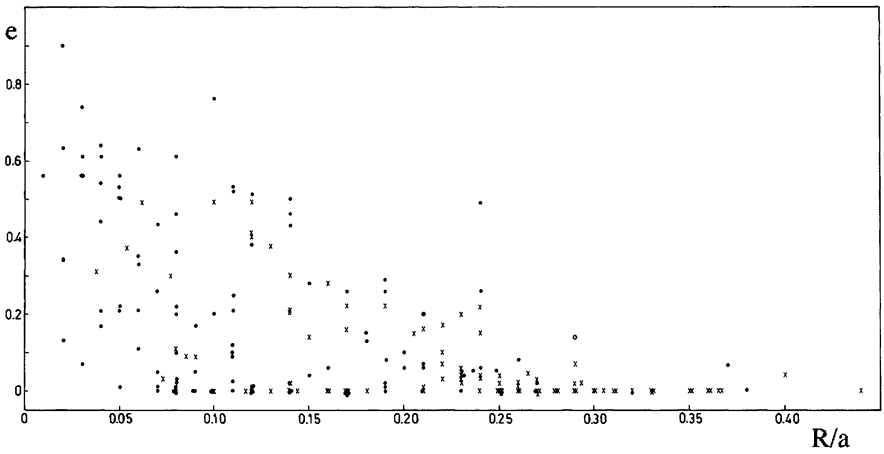

Fig. 8.10 Eccentricity e vs. normalized radius R/a for early-type binaries (spectral types O, B, F) listed in Batten's catalogue (from Giuricin et al. [4]; courtesy A&A)

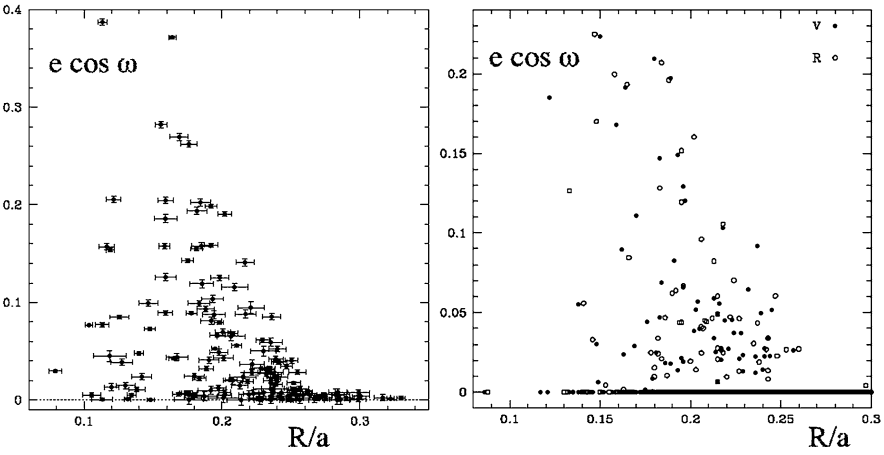

Fig. 8.11 *Left panel*: $e\cos\omega$ vs. relative radius R/a for detached eclipsing binaries in the SMC. *Right panel*: same for the LMC, *full dots* based on *V lightcurves*, *open dots* based on *R lightcurves*. Data from MACHO and OGLE surveys. (From North and Zahn [27]; courtesy A&A)

observed distribution of eccentricities vs. fractional radius displayed in Fig. 8.10, although many binaries are circular for $R/a < 0.25$.

A similar investigation was recently carried out on eclipsing binaries which had been detected in the Magellanic Clouds during the MACHO and OGLE campaigns [27]; the results are shown in Fig. 8.11. Here again the e vs. R/a distribution strongly suggests a transition value of $R/a = 0.255$, in excellent agreement with theory. However an important fraction of binaries are circular at lower fractional radius: it is as if there were two populations of binaries, one complying with the

predictions above, and the other experiencing another, more efficient tidal damping. Histograms of the eccentricity distribution at given R/a confirm that impression, and so does also a much wider survey carried out by Mazeh et al. [24].

On may wonder why the binaries in the Magellanic Clouds behave so similarly to those in our Galaxy: they have lower metallicities, and therefore somewhat larger convective cores, and one would expect that these differences be reflected in the coefficient E_2. However the radii differ too, and the two effects compensate each other such that the predicted transition periods are very nearly the same.

8.5.3 Resonance Locking in Early-Type Binaries

A decade ago, Witte and Savonije [41, 42] revisited the theory of the dynamical tide, by making full account of the Coriolis force. Instead of projecting the forced oscillations on spherical functions, they solved the governing equations directly in two dimensions (r, θ), for various values of the angular velocity Ω and of the tidal frequency $\sigma = j\omega - 2\Omega$ in the rotating frame. When the orbit is circular and the star rotates in the same sense as the orbital motion, only one retrograde mode can be excited at $\sigma = 2\omega - 2\Omega$. But when the orbit is elliptic, many other tidal frequencies appear: $\sigma_j = j\omega - 2\Omega$ with $|j| = 1, 3$, etc. (see Sect. 8.3.5), and both retrograde and prograde modes can be excited. Therefore it is very likely that a binary undergoes some resonances during its evolution, both because the tidal frequency shifts in the course of synchronization, and because the eigenfrequencies are affected by the structural changes of the stars.

In earlier works [6, 34, 45], the effect of resonances on tidal evolution was largely ignored on the belief that stars would move quickly through such resonances, since their width $\Delta\sigma$ is inversely proportional to their amplitude. But Witte and Savonije [42] pointed out that this is not necessarily true, and that a binary can be trapped into a resonance, for elliptic orbits. Retrograde and prograde modes exert torques of opposite sign, and when they balance each other, they may lock the star into such resonances. Moreover, structural changes also can conspire to favor such locking. The consequence is that circularization is sped up by such resonances, as demonstrated by several specific cases they have studied. The results are rather sensitive to the initial conditions, which may explain the observations mentioned above concerning the Magellanic Clouds binaries, namely that for the same orbital period (or fractional radius), some binaries are circular while the others are not, as if there were two tidal damping mechanisms.

8.5.4 Resonance Locking in Late-Type Binaries

Let us come back to the late-type main-sequence binaries. We have seen that turbulent dissipation of the equilibrium tide, at least in its present state, cannot explain the

circularization observed in binaries older than 1 Gyr. This incited Terquem et al. [39] and Goodman and Dickson [8], to examine whether the dynamical tide could not be responsible for the observed circularization. Both teams invoked radiative damping as dissipation mechanism, as had been done previously for early-type stars. But here such damping is rather weak, because the oscillation modes are evanescent in the convection zone, where thermal dissipation would be strongest. Therefore, contrary to what has been found in early type stars, oscillations modes can enter in resonance at very low tidal frequency, i.e. very close to synchronization. This means that one has to deal with modes which have up to thousand radial nodes, which puts a serious burden on the numerical work, as experienced by Terquem et al.; they restricted their exploration to the vicinity of 3 orbital periods, but included turbulent dissipation in the convection zone, where the modes are evanescent. On the contrary, Goodman and Dickson chose a semi-analytical WKB approach, much as in Zahn [46].

Though their quantitative results differ somewhat, the conclusions of the two teams agree, namely that the dynamical tide cannot account for the circularization of the oldest late-type binaries; comparing the predicted transition periods, one sees that it is less efficient than the equilibrium tide.

The problem was re-examined shortly after by Witte and Savonije [43], who anticipated that here also resonance locking could play an important role. Instead of performing the direct 2D calculations as for the early-type binaries, given the high order of the modes, they used the so-called 'traditional approximation', which retains only the radial component of the rotation vector. The r and θ variables then separate again, as in the non-rotating case, the horizontal functions being the so-called Hough functions [35], which contrary to the spherical harmonics depend also on the rotation rate. The tidal torque is displayed in Fig. 8.12, as a function of the forcing frequency.

Today this process of resonance locking in the dynamical tide thus appears as the most efficient process, *on the main-sequence*, among all that have been explored. When starting with quasi-synchronous or super-synchronous stars, the predicted transition period is a slowly increasing function of age; for 5×10^9 yrs, this period is about 7 days, thus higher than that predicted by the equilibrium tide (6 days). But even so, the theoretical predictions are well below the observed ones, unless one allows for very slow, and rather unrealistic initial rotation (such as a period of 100 days). Let us recall that below 1 Gyr the observations agree very well with the transition period derived for the PMS circularization through the equilibrium tide, as we have seen in Sect. 8.4.2

8.6 Tidal Damping Through Inertial Modes

While gravity modes propagate only in stably stratified regions, there is another type of modes, the inertial modes, that are able to propagate also in neutrally stratified convection zones. They owe their existence to the Coriolis force, and hence their frequency, in the frame of the rotating star, is bound by the inertial frequency 2Ω. They may thus be excited by the tidal potential, much as the gravity modes, provided

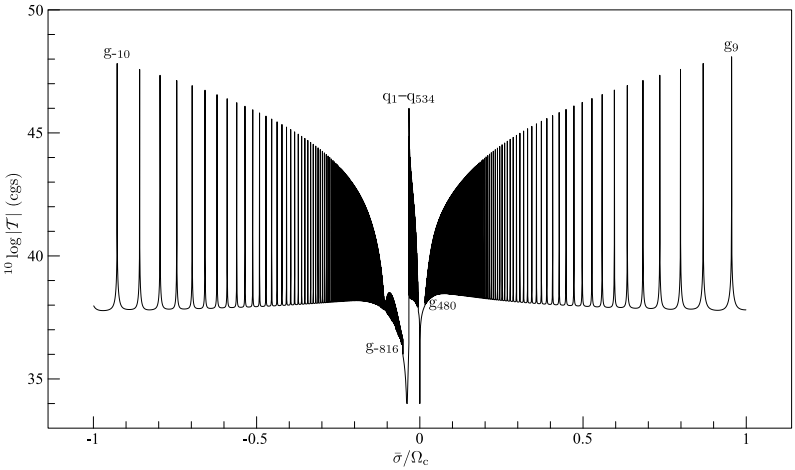

Fig. 8.12 Tidal torque versus forcing frequency $\bar{\sigma}$, scaled by the break-up frequency Ω_c, in a binary of two 1 $M_\odot$ stars, showing the resonances with prograde g-modes ($\bar{\sigma} > 0$), retrograde g-modes ($\bar{\sigma} < 0$), and inertial modes ($-2\Omega < \bar{\sigma} < 0$). (From Savonije and Witte [35]; courtesy A&A)

the tidal frequency is less than the inertial frequency 2Ω. These modes have received little attention so far, until very recently.

Recently Ogilvie and Lin [29] have studied numerically the rôle of these inertial modes in damping the tides, in a solar-type star. The results are depicted in Fig. 8.13. One sees that their contribution (left panel), through their viscous dissipation in the convection zone, can be as large as that of the gravito-inertial modes in the radiation zone (right panel). The dashed lines show the effect of switching off the Coriolis force, and the dotted line, in the left panel, that of increasing the turbulent viscosity by a factor 10. Note that Ogilvie and Lin opted for the quadratic reduction of that turbulent viscosity (Eq. (8.22)), which probably underestimates the contribution of the equilibrium tide.

A remarkable property of these inertial modes is that their peak amplitude, at resonance, does not depend on the strength of the viscosity, as can be seen in the left panel of Fig. 8.13. This is because these modes are described in the inviscid limit by an equation that is spatially hyperbolic, and hence their characteristic rays are focused on wave attractors, where most of viscous dissipation occurs, and whose thickness scales in such a way as to render the dissipation independent of viscosity, as explained in detail by Ogilvie and Lin.

8.7 Conclusion and Perspectives

The reader may wonder why I made no attempt here to reconcile the theoretical predictions for the synchronization of the binary components with their observed

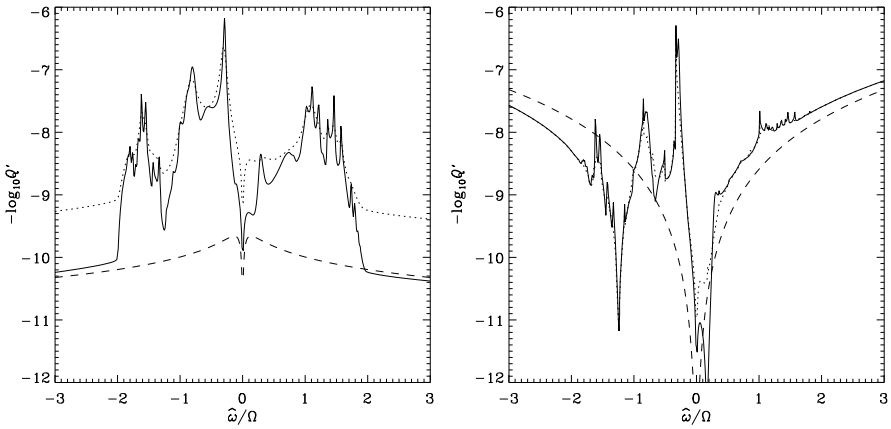

Fig. 8.13 Dissipation rate Q', defined in (8.25) and (8.26), as a function of the tidal frequency $\widehat{\omega}$ normalized by the rotation frequency Ω. The solar model has a spin period of 10 d. *Left*: Q' from the viscous dissipation of inertial modes in the convection zone. *Right*: Q' from the excitation of Hough modes in the radiative zone. The *dashed lines* show the effect of omitting the Coriolis force, hence reducing the dissipation to that of the equilibrium tide. The turbulent viscosity has been reduced according to prescription (8.23). The *dotted lines* show the result of increasing that turbulent viscosity by a factor of 10. (From Ogilvie and Lin [29]; courtesy ApJ)

surface rotation. The reason is that in most cases the tidal torque acts mainly on the outermost part of the star, which is thus synchronized much more rapidly than the interior; therefore the interpretation of the surface rotation requires modeling the transport of angular momentum within the star, in particular where it proceeds at the slowest rate, i.e. in the radiation zones. This is a difficult task that only now begins to be undertaken seriously (cf. [38, 48]), but I am confident that we will see much progress in solving this problem in a not too distant future.

To summarize this review, the two tidal dissipation processes that have received most attention so far are turbulent friction acting on the equilibrium tide, which was first described in the 60s [44], and radiative damping on the dynamical tide, which was identified in the 70s [45]. These processes operate respectively in convection zones and in radiation zones, and they have been quite successful in explaining the observed orbital circularization of binary stars. This is particularly true for the early-type MS binaries, for which we have now at our disposal very large samples gathered during the OGLE and MACHO campaigns: their transition period is precisely defined and it agrees extremely well with that predicted by the theory of the dynamical tide, which is thus validated. However many of these binaries are circularized well above this transition period, as if they had experienced another, more efficient tidal dissipation mechanism. A plausible explanation for this behavior is that these binaries have undergone several episodes of resonance locking, as was described by Witte and Savonije [41, 42].

On the other hand, the equilibrium tide damped by turbulent dissipation accounts very well for the properties of binaries containing a red giant, as was demonstrated by Verbunt and Phinney [40]. It also explains the transition period of about 8 days

observed in late-type binaries that are younger than about 1 Gyr: the explanation is that these have been circularized during the PMS phase, when they were much larger and fully convective. The only serious discrepancy today seems to be the behavior of late-type main-sequence binaries older than 1 Gyr, whose transition period increases with age and is higher than that predicted when applying straightforward the theory of the equilibrium tide. Here again one may invoke the dynamical tide with resonance locking in the radiative core of these stars, as was shown by Witte and Savonije [43].

Their mechanism appears thus highly promising, and it ought to be further explored. For instance, one should take into account that the tidal torque is applied primarily to specific regions: the outer convection zone in late-type MS stars and the outermost part of the radiation zone in early-type stars. These regions are synchronized more quickly than the rest of the star, and therefore differential rotation develops in their radiation zone. This has the effect of increasing the thermal damping, since the local tidal frequency tends then to zero as the tidal wave approaches the synchronized region, as I explained in Sect. 8.5.1.

For late-type binaries, a highly interesting alternative is offered by the damping of inertial waves in their convective envelope, which is being explored by Ogilvie and Lin [29]. This process is likely to play an important role also in giant planets [28]. The difficulty in studying these waves is that they require highly resolved 2D numerical calculations, since the so-called traditional approximation is no longer applicable to render the problem separable.

Work is in progress on several other points, and I shall quote only a few. Kumar and Goodman [15] have studied the enhanced damping of the oscillations triggered in tidal-capture binaries, due to non-linear coupling between the eigenmodes, which is extremely strong in such highly eccentric orbits. Rieutord [33] is examining the possibility that the so-called elliptic instability may occur in binary stars; this instability is observed in the laboratory when the fluid is forced to rotate between boundaries that have a slight ellipticity, and it leads to turbulence [19]. Even the equilibrium tide in late-type binaries is being revisited [32], solving at last the irritating problem of the 'pseudo-resonances' encountered in Zahn [44].

To conclude, I am very pleased to witness this revival of the theory of stellar tides; it owes much to the discovery of extrasolar planets and to the wide surveys mentioned above, which I didn't anticipate forty-five years ago...

References

1. Claret, A., Cunha, N.C.S.: Astron. Astrophys. **318**, 187 (1997)
2. Darwin, G.H.: Philos. Trans. R. Soc. Lond. **170**, 1 (1879)
3. Duquennoy, A., Mayor, M., Mermilliod, J.-C.: In: Duquennoy, A. Mayor, M. (eds.) Binaries as Tracers of Star Formation, p. 52. Cambridge University Press, Cambridge (1992)
4. Giuricin, G., Mardirossian, F., Mezzetti, M.: Astron. Astrophys. **134**, 365 (1984)
5. Goldreich, P., Nicholson, P.D.: Icarus **30**, 301 (1977)
6. Goldreich, P., Nicholson, P.D.: Astrophys. J. **342**, 1079 (1989)
7. Goldreich, P., Soter, S.: Icarus **5**, 375 (1966)

8. Goodman, J., Dickson, E.S.: Astrophys. J. **507**, 938 (1998)
9. Goodman, J., Oh, S.P.: Astrophys. J. **486**, 403 (1997)
10. Hasan, S.S., Zahn, J.-P., Christensen-Dalsgaard, J.: Astron. Astrophys. **444**, L29 (2005)
11. Hut, P.: Astron. Astrophys. **92**, 167 (1980)
12. Hut, P.: Astron. Astrophys. **99**, 126 (1981)
13. Koch, R.H., Hrivnak, B.J.: Astron. J. **86**, 438 (1981)
14. Kopal, Z.: Close Binary Systems. Chapman & Hall, London (1959)
15. Kumar, P., Goodman, J.: Astrophys. J. **466**, 946 (1996)
16. Landsman, W., Aparaicio, J., Bergeron, P., Di Stefano, R., Stecher, T.P.: Astrophys. J. **481**, L93 (1997)
17. Latham, D.W., Mathieu, R.D., Milone, A.E., Davis, R.J.: In Kondo, Y., Sistero, R.F., Polidan, R.S. (eds.) Evolutionary Processes in Interacting Binary Stars. IAU Symp., vol. 151, p. 471. Kluwer Academic, Dordrecht (1992)
18. Latham, D.W., Stefanik, R.P., Torres, G., Davis, R.J., Mazeh, T., Carney, B.W., Laird, J.P., Morse, J.A.: Astron. J. **124**, 1144 (2002)
19. Le Bars, M., Lacaze, L., Le Dizès, S., Le Gal, P., Rieutord, M.: Phys. Earth Planet. Inter. **178**, 48 (2009)
20. Levrard, B., Winidoerfer, C., Chabrier, G.: Astrophys. J. **692**, 9L (2009)
21. Mathieu, R.D., Mazeh, T.: Astrophys. J. **326**, 256 (1988)
22. Mathieu, R.D., Meibom, S., Dolan, C.: Astrophys. J. **602**, 121 (2004)
23. Mayor, M., Mermilliod, J.-C.: In: Maeder, A., Renzini, A. (eds.) Observational Tests of the Stellar Evolution Theory. IAU Symp., vol. 105, p. 411 (1984)
24. Mazeh, T., Tamuz, O., North, P.: Mon. Not. R. Astron. Soc. **367**, 1531 (2006)
25. Melo, C.H.F., Covino, E., Alcalá, J.M., Torres, G.: Astron. Astrophys. **378**, 898 (2001)
26. Mermilliod, J.-C., Rosvick, J.M., Duquennoy, A., Mayor, M.: Astron. Astrophys. **265**, 513 (1992)
27. North, P., Zahn, J.-P.: Astron. Astrophys. **405**, 677 (2003)
28. Ogilvie, G.I., Lin, D.N.C.: Astrophys. J. **610**, 477 (2004)
29. Ogilvie, G.I., Lin, D.N.C.: Astrophys. J. **661**, 1180 (2007)
30. Penev, K., Sasselov, D., Robinson, F., Demarque, P.: Astrophys. J. **655**, 1166 (2007)
31. Penev, K., Sasselov, D., Robinson, F., Demarque, P.: Astrophys. J. **704**, 930 (2009)
32. Remus, F., Mathis, S., Zahn, J.-P.: Astron. Astrophys. **544**, 132 (2012)
33. Rieutord, M.: In: Eennens, Ph., Maeder, A. (eds.) Stellar Rotation. IAU Symp., vol. 215, p. 394 (2004)
34. Rocca, A.: Astron. Astrophys. **213**, 114 (1989)
35. Savonije, G.J., Witte, M.G.: Astron. Astrophys. **386**, 111 (2002)
36. Stahler, S.W.: Astrophys. J. **274**, 822 (1983)
37. Stahler, S.W.: Astrophys. J. **332**, 804 (1988)
38. Talon, S.: EAS Publ. Ser. **32**, 81 (2008)
39. Terquem, C., Papaloizou, J.C.B., Nelson, R.P., Lin, D.N.C.: Astrophys. J. **502**, 788 (1998)
40. Verbunt, F., Phinney, E.S.: Astron. Astrophys. **296**, 709 (1995)
41. Witte, M.G., Savonije, G.J.: Astron. Astrophys. **341**, 842 (1999)
42. Witte, M.G., Savonije, G.J.: Astron. Astrophys. **350**, 129 (1999)
43. Witte, M.G., Savonije, G.J.: Astron. Astrophys. **386**, 222 (2002)
44. Zahn, J.-P.: Ann. Astrophys. **29**, 489 (1966)
45. Zahn, J.-P.: Astron. Astrophys. **41**, 329 (1975)
46. Zahn, J.-P.: Astron. Astrophys. **57**, 383 (1977)
47. Zahn, J.-P.: Astron. Astrophys. **220**, 112 (1989)
48. Zahn, J.-P.: EAS Publ. Ser. **26**, 49 (2007)
49. Zahn, J.-P., Bouchet, L.: Astron. Astrophys. **223**, 112 (1989)